

Superconductivity with T_c up to 30.7 K in air-annealed CaFeAsF

Yixin Liu^{1,2}, Teng Wang^{1,3}, Zulei Xu^{1,2}, Da Jiang^{1,4}, Yi Zhao³, Yanpeng Qi^{3,5,6}, Xiaoni Wang^{1,2}, Ming Yang^{1,7}, Mao Ye^{1,2}, Wei Peng^{1,2}, and Gang Mu^{1,2,†}

Exploring new unconventional superconductors is of great value for both fundamental research and practical applications. It is a long-term challenge to develop and study more hole-doped superconductors in 1111 system of iron-based superconductors. However, fifteen years after the discovery of iron-based superconductors, it has become increasingly difficult to discover new members in this system by conventional means. Here we report the discovery of superconductivity with the critical transition temperature up to 30.7 K in the parent compound CaFeAsF by an annealing treatment in air atmosphere. The superconducting behaviors are verified in both the single-crystalline and polycrystalline samples by the resistance and magnetization measurements. The analysis by combining the depth-resolved time-of-flight secondary ion mass spectrometry (TOF-SIMS) and X-ray photoelectron spectroscopy (XPS) measurements show that the introduction of oxygen elements and the consequent changing in Fe valence by the annealing treatment may lead to the hole-type doping, which is the origin for the occurrence of superconductivity. Our result paves the way for further in-depth investigations on the hole-doped 1111 system in iron-based superconductors.

¹National Key Laboratory of Materials for Integrated Circuits, Shanghai Institute of Microsystem and Information Technology, Chinese Academy of Sciences, Shanghai 200050, China. ²University of Chinese Academy of Sciences, Beijing 100049, China. ³School of Physical Science and Technology, ShanghaiTech University, Shanghai 201210, China. ⁴Institute for Frontiers and Interdisciplinary Sciences, Zhejiang University of Technology, Hangzhou 310014, China. ⁵ShanghaiTech Laboratory for Topological Physics, ShanghaiTech University, Shanghai 201210, China. ⁶Shanghai Key Laboratory of High-resolution Electron Microscopy, ShanghaiTech University, Shanghai 201210, China. ⁷School of Microelectronics, Shanghai University, Shanghai 200444, China. Correspondence and requests for materials should be addressed to G.M. (email: mugang@mail.sim.ac.cn).

As the second class of high-temperature superconducting system after copper-based superconductors in terms of critical transition temperature (T_c) at ambient pressure, iron-based superconductors (IBSs)¹ show great potential in both basic research²⁻⁵ and practical applications⁶. In general, the discovery of new superconductors in the field of unconventional superconductivity often leads to unexpected new insights into the physics of superconductivity. For example, the discovery of superconductivity in $A_x\text{Fe}_{2-y}\text{Se}_2$ ($A = \text{K, Rb, Tl}$)^{7,8} and monolayer FeSe on SrTiO_3 ⁹ led to the realization that superconductivity with relatively high- T_c may also exist in systems where the hole-type Fermi surface disappears completely¹⁰⁻¹² and the Fermi surface nesting is not the key factor for occurrence of high- T_c superconductivity in this system¹³. After fifteen years of continuous efforts, a wide variety of iron-based superconducting materials with different crystal structures and T_c have been discovered^{7-9, 14-22}. To date, it has become increasingly difficult to discover new superconductors in this system by conventional means, both in terms of new structures and new ways of inducing superconductivity (including chemical doping, pressurization, etc.).

It's worth drawing our attention to the 1111 system ReFeAsO ($\text{Re} = \text{rare-earth element}$), which is the earliest discovered subclass¹ and reveals the highest T_c ($\approx 55 \text{ K}$)¹⁵ in the bulk materials of the IBSs. Both electron-^{1, 14, 15} and hole-doping²³⁻²⁵ can induce superconductivity by substituting F and Sr to the site of O and rare earth elements, respectively. A noteworthy state of affairs is that the materials and the research on the hole-doping side are relatively rare. To develop more hole-doped superconductors in 1111 system of iron-based superconductors is a long-term challenge. On the other hand, due to the successful acquisition of high-quality single-crystalline samples^{26, 27}, people have carried out in-depth and extensive research on the fluoride-based 1111-

type compound CaFeAsF in recent years²⁸⁻³⁵. Typically superconductivity can be induced by chemical doping (e.g. $\text{Ca}_{1-x}\text{Nd}_x\text{FeAsF}$ ³⁶ and $\text{CaFe}_{1-x}\text{Co}_x\text{AsF}$ ³⁷) or applying pressure^{38,39}. Unfortunately, currently only the Co-doped compound $\text{CaFe}_{1-x}\text{Co}_x\text{AsF}$ can be grown into single-crystalline samples²⁷. Since the dopant Co is doped at the Fe site, the maximum value of T_c is only 21 K in this material. Therefore, it is still necessary to explore new superconducting materials with higher T_c and/or different doping types in this system.

In this paper, we report a new route to induce superconductivity from the parent phase CaFeAsF by the annealing treatment. The superconductivity with maximum critical transition temperature of 30.7 K is verified by both the resistance and magnetization measurements in the samples annealed in air atmosphere. The maximum SC volume fraction is 20.5% by the annealing treatment at 380 °C for 12 hrs. The upper critical field and its anisotropy are investigated by the resistance measurements under magnetic field. Further analysis combined with the depth-resolved TOF-SIMS and XPS measurements showed that the oxygen and fluorine contents of the annealed samples changed significantly within about 1000 seconds of etching, accompanied by an increase in the valence of Fe element. We argue that the involving of oxygen element and the changing in Fe valence is very likely to cause the hole-doping in CaFeAsF, which is the origin for the observed superconductivity in this system.

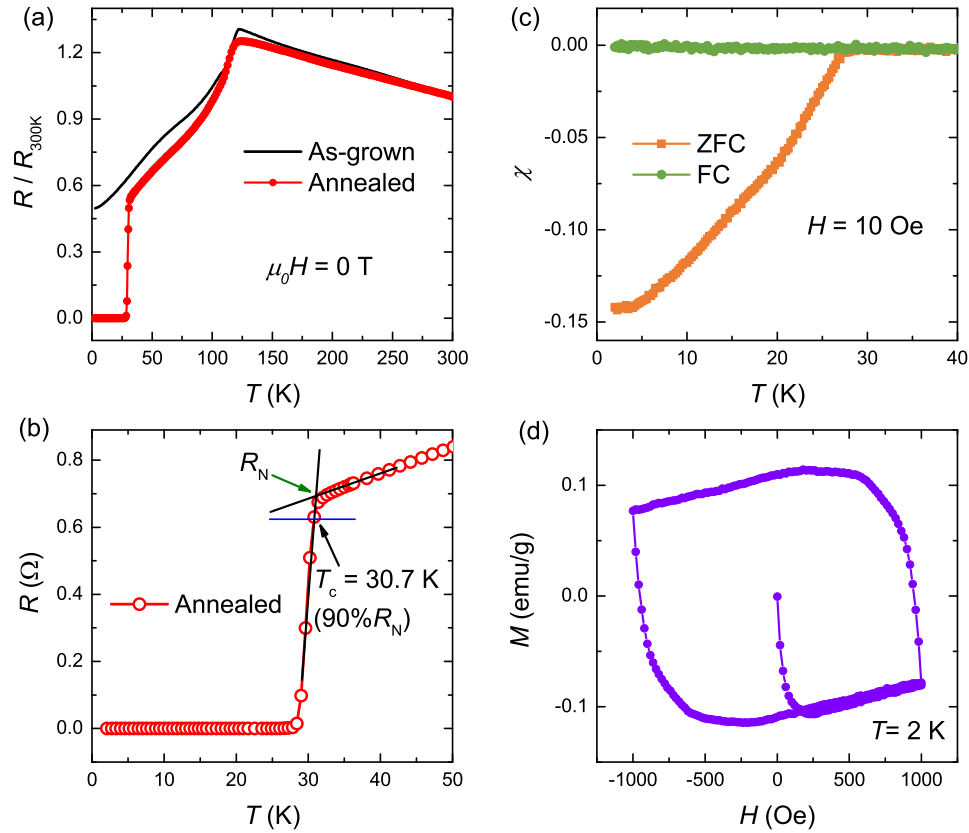


Figure 1 Superconductivity in single-crystalline CaFeAsF annealed in air atmosphere.

(a) Temperature dependence of normalized resistance of the as-grown (black) and annealed (red) CaFeAsF single crystals under zero magnetic field. (b) Resistance data of the annealed samples in the low temperature region. The arrowed lines indicated the criterion in determining the critical transition temperature T_c . (c) Magnetic susceptibility of the annealed sample measured in zero-field-cooled (ZFC) and field cooled (FC) modes. (d) The isothermal hysteresis loop of magnetization for the annealed sample at 2 K.

Results

The X-ray diffraction (XRD) data (see SI) show that both annealed and as-grown samples exhibit good crystallinity. As shown in Fig. 1(a), normalized resistance of the CaFeAsF single crystal, which has been annealed at 330 °C for 18 hrs, undergoes a clear and sharp superconducting transition in the low-temperature region. Meanwhile, the $R/R_{300K}-T$ curve roughly follow a similar trace with that of the as-grown CaFeAsF in the high-temperature region, which reveals a structure transition at around 121 K. Such a behavior indicates the coexistence of superconductivity and parent phase in the annealed sample. In order to have a clearer view of the superconducting transition, we show the resistance in the low temperature region in Fig. 1(b). Using a criterion of 90% R_n , where R_n is the normal-state resistance before SC transition, the onset transition temperature T_c is determined to be 30.7 K. We note that such a value is about 10 K higher than that observed in Co-doped CaFeAsF^{27,37}. The occurrence of superconductivity is further confirmed by the magnetic susceptibility (χ) measurements, see Fig. 1(c). The magnetic field was applied parallel to the ab -plane of the crystal to minimize the effect of the demagnetization effect. The onset transition point in the $\chi-T$ curve is 27.5 K, which is very close to the zero-resistance temperature. The SC volume fraction of this samples is about 14.2%, which is consistent with the inference from the normal-state resistance data (see Fig. 1(a)) that the SC state coexists with the parent phase of CaFeAsF. The $M-H$ curve measured at 2 K shows a typical hysteresis loop of the type-II superconductors (see Fig. 1(d)).

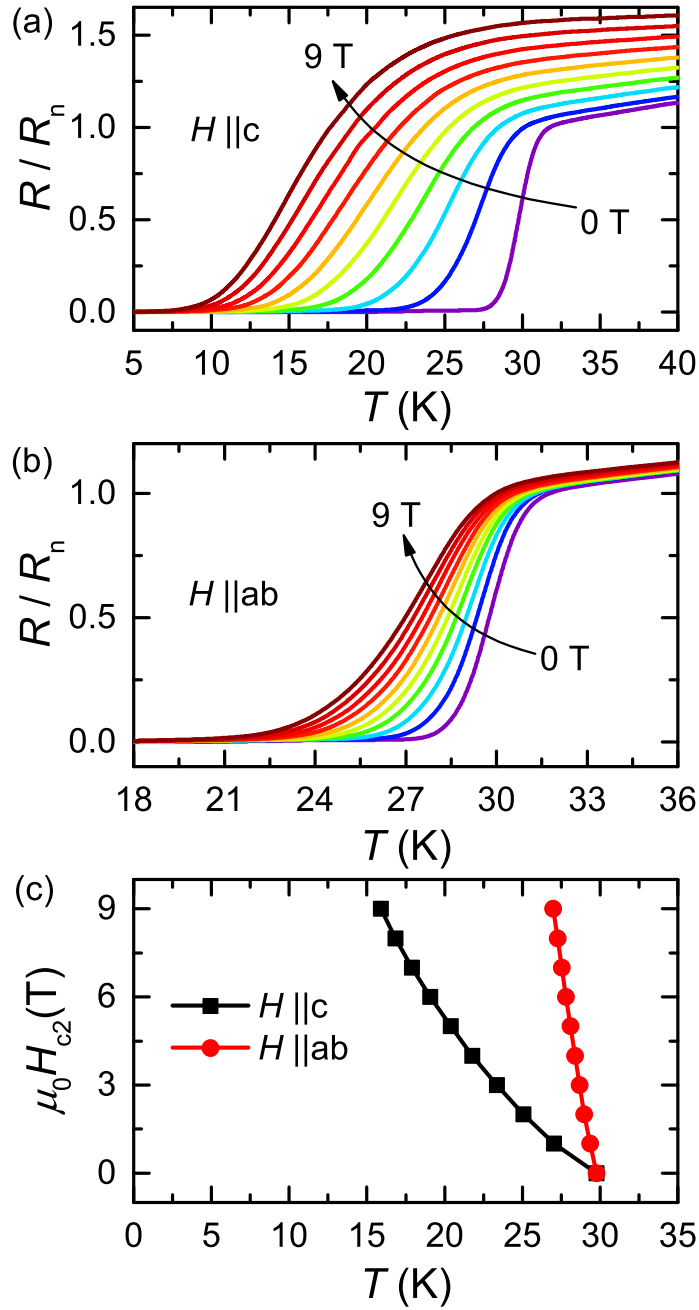


Figure 2 Upper critical field of annealed CaFeAsF single crystals. (a, b) The normalized resistance as a function of temperature under the magnetic field up to 9 T with $H \parallel c$ and

$H \parallel ab$, respectively. The interval of the magnetic field is 1 T. (c) Upper critical fields $\mu_0 H_{c2}$ as a function of temperature for two field orientations.

To study the upper critical field and its anisotropy, we performed the measurements on the temperature dependence of electrical transport with the magnetic field along two different orientations: $H \parallel c$ and $H \parallel ab$. As shown in Figs. 2(a) and (b), for both field orientations, the SC transition point shifts to lower temperature with the increase of the magnetic field. It is notable that such a shift is much more quickly when the magnetic field is applied along the c axis, revealing a significant anisotropic characteristic. Using the criteria of $50\% \rho_n$, the values of upper critical $\mu_0 H_{c2}$ are extracted, see Fig. 2(c). The $\mu_0 H_{c2}-T$ data reveals a steeper slope near T_c with $H \parallel ab$ than that with $H \parallel c$, further verifies the anisotropic feature of the upper critical field. Quantitatively, the slope of the tangent in the $H_{c2}-T$ curves near T_c , $d\mu_0 H_{c2}/dT|_{T_c}$, is -2.53 and -0.36 T/K for the orientations of $H \parallel ab$ and $H \parallel c$ respectively, which gives rise to an anisotropy parameter of $\Gamma = 7$. We note that this value is smaller than that reported in Co-doped CaFeAsF,³⁰ indicating the differences in electronic structure of the present annealed system as compared with the Co-doped one.

In general, polycrystalline materials have smaller grains and larger specific surface areas than single-crystalline ones. Therefore, in order to improve the efficiency of annealing treatment and to increase the SC volume fraction, we also carried out annealing experiments in air atmosphere in polycrystalline materials. The powder X-ray diffraction patterns of annealed samples and the magnetic properties of the untreated sample can be seen in SI. The positions of diffraction peaks of

the CaFeAsF phase remain almost unchanged for the annealed sample, as compared with the untreated ones. The temperature dependence of χ reveals a systematic evolution with annealing temperature T_{ann} and time, see Fig. 3(a) for the ZFC mode. When $T_{ann} = 300$ °C, superconductivity begins to emerge, although with a rather low T_c and small SC volume fraction. The maximum value of T_c at around 27.7-28.5 K can be achieved when 350 °C $\leq T_{ann} \leq 410$ °C. The χ - T data with FC mode can be seen in the inset of Fig. 3(a), taking one of the samples as an example. The superconductivity is also confirmed by the M - H curve, as can be seen in Fig. 3(b).

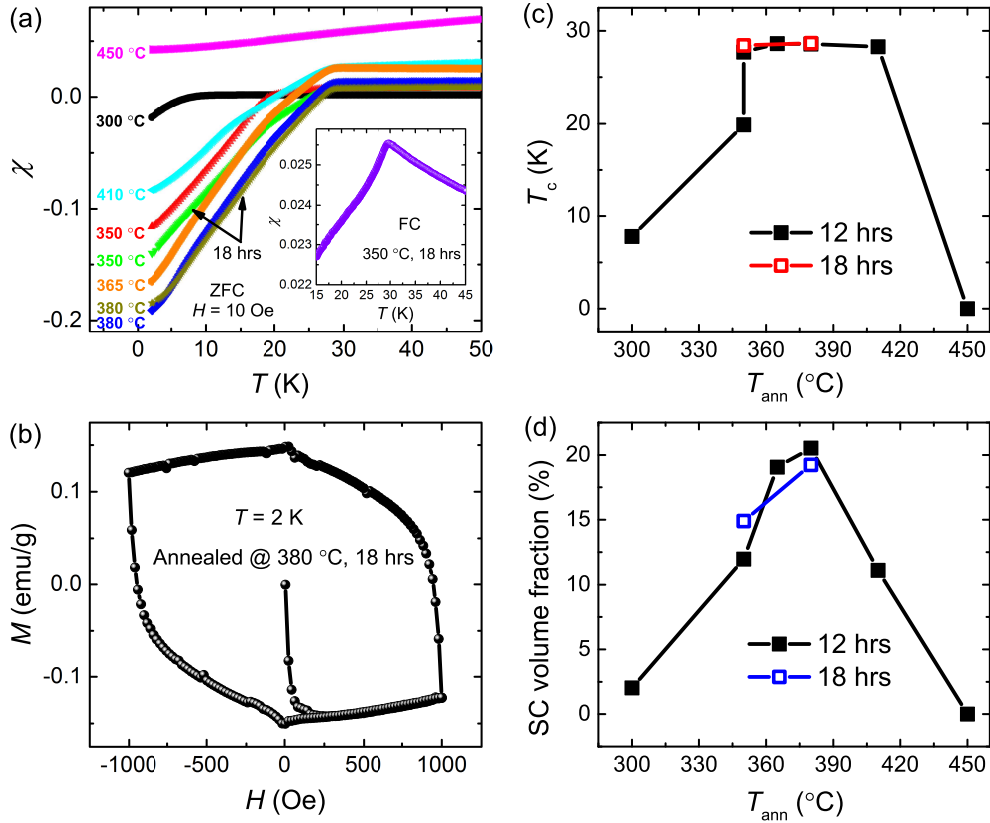


Figure 3 Superconductivity in polycrystalline CaFeAsF samples annealed under vari-

ous conditions in air atmosphere. (a) Magnetic susceptibility of the annealed samples measured with ZFC mode. The annealing time is 12 hrs, except for the two curves indicated by the arrows (18 hrs). The inset show the data with FC mode for one sample as an example. (b) The isothermal hysteresis loop of magnetization for the sample annealed at 380 °C for 18 hrs. (c, d) Superconducting critical transition temperature and the SC volume fraction as a function of the annealing temperature.

In Figs. 3(c) and (d), we summarized the values of T_c and SC volume fraction as a function of the annealing temperature T_{ann} derived from the data in Fig. 3(a). It can be seen that, for the highest superconducting transition temperature, there is a wide temperature window in the annealing conditions; while the SC volume fraction shows a peak shape versus the annealing temperature. Combining these two factors, the optimal annealing condition for the polycrystalline samples is 365-380 °C and 12 hrs. It is worth noting that the highest superconducting volume fraction in the annealed polycrystalline samples is 20.5%, which is significantly higher than the value obtained in the single-crystalline samples ($\sim 14.2\%$). This confirms our previous speculation that the structural characteristics of polycrystalline materials allow them to exhibit more pronounced annealing effects.

Discussion

It is obviously necessary to reveal the internal mechanism of the superconductivity in the present annealed CaFeAsF system. In order to achieve this goal, we have carried out relevant experimental research. Firstly, the annealing gas components that are decisive for the generation of supercon-

ductivity are carefully identified. Besides the air atmosphere, we checked the annealing effect of CaFeAsF single crystal in high purity oxygen (O_2), the mixture of nitrogen and oxygen that mimics the proportions of air (N_2+O_2), and carbon dioxide gas (CO_2). The magnetization data can be seen in SI. Here we summarize the main result of the annealing effect in different atmospheres in Table 1. It can be seen that the mixture of N_2 and O_2 has a similar effect with air and the annealing in CO_2 could not induce superconductivity. Moreover, annealing in purity O_2 can also lead to the occurrence of superconductivity, although with a relatively lower T_c and SC volume fraction. Meanwhile, elemental analysis combined with TOF-SIMS and XPS measurements showed that there was no nitrogen elements present in the annealed samples. Combining these information, we preliminarily deduce that the introduction of oxygen element during the annealing process may be a key factor in the generation of superconductivity.

Table 1: Summary of the annealing effect on CaFeAsF single crystals in different atmospheres. All the samples were annealed under the same temperature and time (330 °C for 18 hrs).

Atmosphere	Air	O_2	N_2+O_2	CO_2
T_c ^a	27.5	11.2	24.5	Non-SC ^b
SC volume fraction	14.2%	7.7%	14.1%	Non-SC

^a Here the values of T_c are determined from the χ - T data. ^b Non-SC is an abbreviation of non-superconducting.

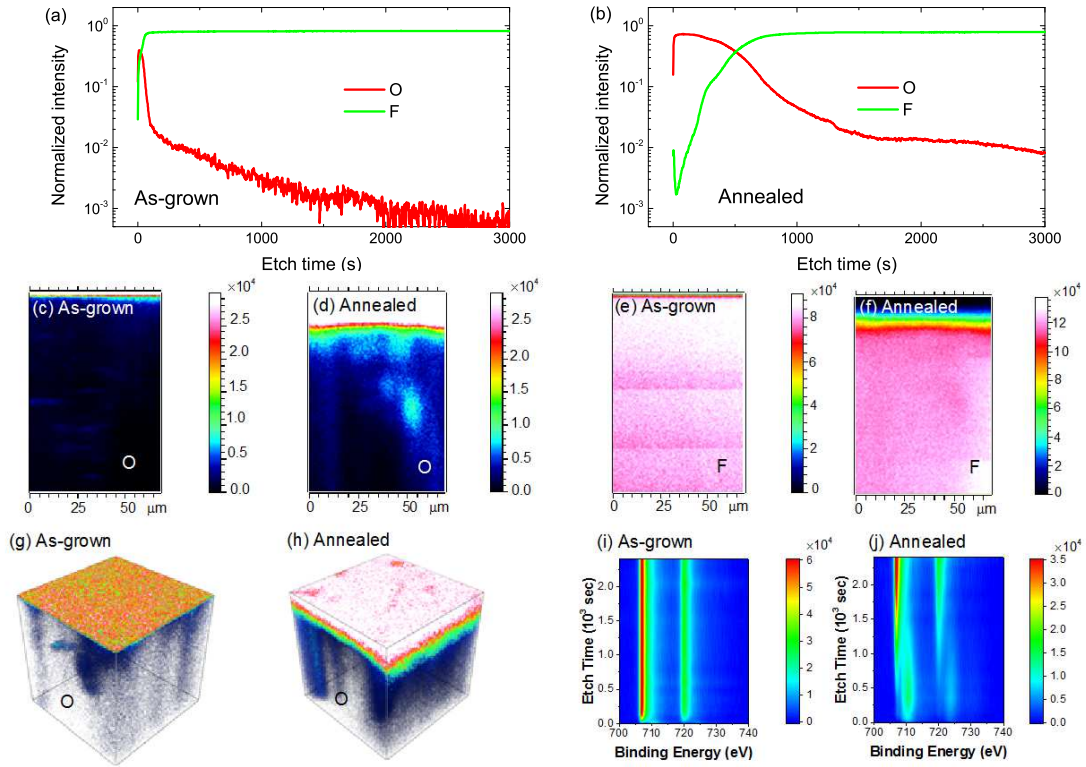


Figure 4 Depth analysis of elemental content and energy spectrum characterization in the single-crystalline samples. (a, b) Normalized intensity of O and F elements as a function of the etch time (a indicator for the depth from samples surface) for the as-grown and annealed samples from the TOF-SIMS measurements, respectively. (c, d) The cross-section images of the TOF-SIMS intensity (unit: counts) of oxygen element for the as-grown and annealed samples respectively. (e, f) The cross-section images of the TOF-SIMS intensity (unit: counts) of fluorine element for the as-grown and annealed samples respectively. (g, h) The three-dimensional images of the TOF-SIMS intensity (unit: counts) of oxygen element for the as-grown and annealed samples respectively. (i, j) Colormaps

of the XPS spectra (unit: counts/s) of Fe 2p state for the as-grown and annealed samples respectively in a wide range of etch time.

To further corroborate our inferences, we examined the depth-resolved element content on both as-grown and annealed samples by means of time-of-flight secondary ion mass spectrometry (TOF-SIMS). The information at different depth of the single-crystalline samples was collected by etching the samples controllably using cesium ions. For the as-grown sample, the oxygen content had dropped to 2% of the total amount with an etch time of 120 seconds (see Fig. 4(a)). In stark contrast, the annealed sample needed to be etched for more than 1300 seconds before the oxygen content dropped to the same level (see Fig. 4(b)). This result gives the direct evidence that oxygen is introduced into samples during the annealing process. Moreover, the evolution of fluorine content with depth generally shows the opposite trend to oxygen. This indicates that the oxygen element introduced in the annealing process is mainly in competition with fluorine. The cross-section images for the distributions of oxygen and fluorine in as-grown and annealed samples shown in Figs. 4(c), (d), (e), and (f) respectively give the more intuitive representations of this evolutionary trend. In Figs. 4(g) and (h), we also display the three-dimensional images of the TOF-SIMS intensity of oxygen, which reflects the element content, of the as-grown and annealed samples respectively. From the information of etch time, we can roughly estimate that the oxygen content affects the range of about 150 nm from the sample surface. This may explain why no shift was seen in the peak positions of the XRD data in the annealed samples, since the detection depth of the XRD measurement is typically in the order of a few to tens of microns.

Finally, the valence of Fe ions was investigated using X-ray photoelectron spectroscopy (XPS). The samples were etched using argon ion with the energy of 1 keV. As can be seen in Fig. 4(i), there are two main peaks located at 706.9 and 720.0 eV in the XPS spectrum of the as-grown sample, reflecting the Fe 2p_{3/2} and 2p_{1/2} states respectively. For the annealed sample, in addition to the two peaks observed in the as-grown sample, two peaks at slightly higher energy positions appeared on the XPS spectrum at 710.5 and 723.5 eV when etch time of the ion beam was below about 1000 seconds. It is worth noting that, due to the unavoidable reduction during the ion etching process, it is not yet possible to derive the precise value of Fe valence from the peak position we have obtained. Nevertheless, the qualitative trend is certain, that is, the annealing treatment raises the valence of Fe element. Based on this experimental fact, we can further infer that the introduction of oxygen elements during the annealing process probably brought about hole-doping to CaFeAsF. And this, in turn, is the reason for the appearance of superconductivity in this system. In this sense, the T_c of the hole-doped material in iron-based superconducting 1111-system has been increased from the previous 25 K in $\text{La}_{1-x}\text{Sr}_x\text{FeAsO}^{23}$ to the present 30.7 K. Of course, the presence of hole-type doping needs to be confirmed by Hall effect measurements after pure superconducting samples (without the parent phase) are obtained in the future.

In summary, we discovered superconductivity with T_c up to 30.7 K in air-annealed CaFeAsF. The maximum superconducting volume fraction is 20.5% in the polycrystalline samples annealed at 380 °C for 12 hrs. The single-crystalline sample revealed an anisotropy of $\Gamma = 7$ for the upper critical field. Comparative experiments of annealing treatments under various atmospheres and characterization analysis combining TOF-SIMS and XPS indicate that the introduction of oxygen

during annealing and the concomitant elevation of Fe valence are likely to be the key reasons for the generation of superconductivity. Our findings are likely to developed a new type of hole-doped superconductivity in the 1111 system, whose T_c has exceeded that reported previously.

Experimental Section

Sample preparation and annealing. The CaFeAsF single crystals were grown by the self-flux method. The detailed growth process has been reported in the previous work²⁶. The polycrystalline samples were prepared using the solid-state reaction at 1010 °C for 40 hrs. The single-crystalline sample were annealed in different atmospheres, including air, O₂, the mixture of N₂ and O₂ that mimics the proportions of air, and CO₂, at 330 °C for 18 hrs. For the polycrystalline samples, the annealing temperature ranges from 300 to 450 °C. Two different annealing times were adopted: 12 and 18 hrs.

Characterization. The The crystal structure of the CaFeAsF samples, including single-crystalline and polycrystalline ones, were examined by a DX-2700-type X-ray diffractometer using Cu K_α radiation. The element contents were measure using the time-of-flight secondary ion mass spectrometry (ION-TOF GmbH, TOF-SIMS 5-100). The valence of Fe elements was evaluated using the X-ray photoelectron spectroscopy (Thermo Fisher Scientific, Escalab 250Xi). To obtain depth dependence of information, the single-crystalline samples were etched using Cs and Ar ions when carrying out TOF-SIMS and XPS measurements respectively. In the TOF-SIMS measurements, the etch area is $180 \times 180 \mu\text{m}^2$. The energy of the ion beam is 1 keV. The microstructure of the single-crystalline samples was characterized by the Cs-corrected transmission electron microscopy

(JEOL, JEM-ARM300F).

Electrical transport and magnetization measurements. The electrical resistance were measured on the physical property measurement system (Quantum Design, PPMS) by a standard four-probe method. The silver paste was used to fabricate the electrodes. The external magnetic field of up to 9 T was applied in two orientations ($H \parallel c$ and $H \parallel ab$) and perpendicular to the electric current. The magnetization measurements were carried out on the magnetic property measurement system (Quantum Design, MPMS 3). For the magnetization measurements on single-crystalline samples, the magnetic field was applied parallel to the ab -plane to minimize the effect of the demagnetization effect.

Supporting Information

Supporting Information is available from the Wiley Online Library or from the author.

Acknowledgments

This work is supported by the National Natural Science Foundation of China (Nos. 11204338 and 52272265), National Key R&D Program of China (No. 2018YFA0704300), and the Youth Innovation Promotion Association of the Chinese Academy of Sciences (No. 2015187). The experimental measurements were supported by the Superconducting Electronics Facility (SELF) of Shanghai Institute of Microsystem and Information Technology.

Conflict of Interest

The authors declare no conflict of interest.

Keywords

Iron-based superconductor, CaFeAsF, Annealing treatment, Unconventional superconductivity

References

1. Kamihara, Y., Watanabe, T., Hirano, M. & Hosono, H. Iron-based layered superconductor La[O_{1-x}F_x]FeAs (x = 0.05-0.12) with $T_c = 26$ K. *J. Am. Chem. Soc.* **130**, 3296–3297 (2008).
2. Si, Q. & Abrahams, E. Strong correlations and magnetic frustration in the high T_c iron pnictides. *Phys. Rev. Lett.* **101**, 076401 (2008).
3. Hirschfeld, P. J., Korshunov, M. M. & Mazin, I. I. Gap symmetry and structure of Fe-based superconductors. *Rep. Prog. Phys.* **74**, 124508 (2011).
4. Johnston, D. C. The puzzle of high temperature superconductivity in layered iron pnictides and chalcogenides. *Adv. Phys.* **59**, 803–1061 (2010).
5. Hosono, H. & Kuroki, K. Iron-based superconductors: Current status of materials and pairing mechanism. *Physica C* **514**, 399–422 (2015).
6. Hosono, H., Yamamoto, A., Hiramatsu, H. & Ma, Y. Recent advances in iron-based superconductors toward applications. *Mater. Today* **21**, 278–302 (2018).

7. Guo, J. *et al.* Superconductivity in the iron selenide $K_xFe_2Se_2$ ($0 \leq x \leq 1.0$). *Phys. Rev. B* **82**, 180520 (2010).
8. Fang, M.-H. *et al.* Fe-based superconductivity with $T_c = 31$ K bordering an antiferromagnetic insulator in $(Tl,K)Fe_xSe_2$. *Europhys. Lett.* **94**, 27009 (2011).
9. Wang, Q.-Y. *et al.* Interface-induced high-temperature superconductivity in single unit-cell FeSe films on SrTiO₃. *Chin. Phys. Lett.* **29**, 037402 (2012).
10. Zhang, Y. *et al.* Nodeless superconducting gap in $A_xFe_2Se_2$ ($A = K, Cs$) revealed by angle-resolved photoemission spectroscopy. *Nat. Mater.* **10**, 273 (2011).
11. Wang, X.-P. *et al.* Strong nodeless pairing on separate electron fermi surface sheets in $(Tl, K)Fe_{1.78}Se_2$ probed by ARPES. *Europhys. Lett.* **93**, 57001 (2011).
12. Mou, D. *et al.* Distinct fermi surface topology and nodeless superconducting gap in a $(Tl_{0.58}Rb_{0.42})Fe_{1.72}Se_2$ superconductor. *Phys. Rev. Lett.* **106**, 107001 (2011).
13. Hu, J. P. & Ding, H. Local antiferromagnetic exchange and collaborative fermi surface as key ingredients of high temperature superconductors. *Sci. Rep.* **2**, 381 (2012).
14. Chen, X. H. *et al.* Superconductivity at 43 K in $SmFeAsO_{1-x}F_x$. *Nature* **453**, 761–762 (2008).
15. Ren, Z.-A. *et al.* Superconductivity at 55 K in iron-based F-doped layered quaternary compound $Sm[O_{1-x}F_x]FeAs$. *Chin. Phys. Lett.* **25**, 2215 (2008).
16. Wang, X. *et al.* The superconductivity at 18 K in LiFeAs system. *Solid State Commun.* **148**, 538–540 (2008).

17. Tapp, J. H. *et al.* LiFeAs: An intrinsic FeAs-based superconductor with $T_c = 18$ K. *Phys. Rev. B* **78**, 060505 (2008).
18. Hsu, F.-C. *et al.* Superconductivity in the PbO-type structure α -FeSe. *Natl. Acad. Sci.* **105**, 14262–14264 (2008).
19. Rotter, M., Tegel, M. & Johrendt, D. Superconductivity at 38 K in the iron arsenide $\text{Ba}_{1-x}\text{K}_x\text{Fe}_2\text{As}_2$. *Phys. Rev. Lett.* **101**, 107006 (2008).
20. Qi, Y. *et al.* Superconductivity at 34.7 K in the iron arsenide $\text{Eu}_{0.7}\text{Na}_{0.3}\text{Fe}_2\text{As}_2$. *New J. Phys.* **10**, 123003 (2008).
21. Zhu, X. *et al.* Transition of stoichiometric $\text{Sr}_2\text{VO}_3\text{FeAs}$ to a superconducting state at 37.2 K. *Phys. Rev. B* **79**, 220512(R) (2009).
22. Wang, Z.-C. *et al.* Superconductivity in $\text{KCa}_2\text{Fe}_4\text{As}_4\text{F}_2$ with separate double Fe_2As_2 layers. *J. Am. Chem. Soc.* **138**, 7856–7859 (2016).
23. Wen, H. H., Mu, G., Fang, L., Yang, H. & Zhu, X. Superconductivity at 25 K in hole-doped $(\text{La}_{1-x}\text{Sr}_x)\text{OFeAs}$. *Europhys. Lett.* **82**, 17009 (2008).
24. Kasperkiewicz, K., Bos, J.-W. G., Fitch, A. N., Prassides, K. & Margadonna, S. Structural and electronic response upon hole doping of rare-earth iron oxyarsenides $\text{Nd}_{1-x}\text{Sr}_x\text{FeAsO}$ ($0 < x \leq 0.2$). *Chem. Commun.* 707–709 (2009).
25. Mu, G. *et al.* Synthesis, structural, and transport properties of the hole-doped superconductor $\text{Pr}_{1-x}\text{Sr}_x\text{FeAsO}$. *Phys. Rev. B* **79**, 104501 (2009).

26. Ma, Y. H. *et al.* Growth and characterization of millimeter-sized single crystals of CaFeAsF. *Supercond. Sci. Technol.* **28**, 085008 (2015).
27. Ma, Y. H. *et al.* Growth and characterization of CaFe_{1-x}Co_xAsF single crystals by caas flux method. *J. Cryst. Growth* **451**, 161 (2016).
28. Terashima, T. *et al.* Fermi surface with Dirac fermions in CaFeAsF determined via quantum oscillation measurements. *Phys. Rev. X* **8**, 011014 (2018).
29. Xiao, H. *et al.* Superconducting fluctuation effect in CaFe_{0.88}Co_{0.12}AsF. *J. Phys.: Condens. Matter* **28**, 455701 (2016).
30. Ma, Y. H. *et al.* Strong anisotropy effect in iron-based superconductor CaFe_{0.882}Co_{0.118}AsF. *Supercond. Sci. Technol.* **30**, 074003 (2017).
31. Xu, B. *et al.* Optical study of Dirac fermions and related phonon anomalies in the antiferromagnetic compound CaFeAsF. *Phys. Rev. B* **97**, 195110 (2018).
32. Ma, Y. H. *et al.* Magnetic-field-induced metal-insulator quantum phase transition in CaFeAsF near the quantum limit. *Sci. China Phys. Mech.* **61**, 127408 (2018).
33. Mu, G. & Ma, Y. Single crystal growth and physical property study of 1111-type Fe-based superconducting system CaFeAsF. *Acta Phys. Sin.* **67**, 177401 (2018).
34. Terashima, T., Uji, S., Wang, T. & Mu, G. Topological frequency shift of quantum oscillation in CaFeAsF. *npj Quantum Mater.* **7**, 25 (2022).

35. Terashima, T. *et al.* Anomalous high-field magnetotransport in CaFeAsF due to the quantum hall effect. *npj Quantum Mater.* **7**, 62 (2022).
36. Cheng, P. *et al.* High- T_c superconductivity induced by doping rare-earth elements into CaFeAsF. *Europhys. Lett.* **85**, 67003 (2009).
37. Matsuishi, S. *et al.* Effect of 3d transition metal doping on the superconductivity in quaternary fluoroarsenide CaFeAsF. *New J. Phys.* **11**, 025012 (2009).
38. Okada, H. *et al.* Pressure dependence of the superconductor transition temperature of $\text{Ca}(\text{Fe}_{1-x}\text{Co}_x)\text{AsF}$ compounds: A comparison with the effect of pressure on $\text{LaFeAsO}_{1-x}\text{F}_x$. *Phys. Rev. B* **81**, 054507 (2010).
39. Gao, B., Ma, Y., Mu, G. & Xiao, H. Pressure-induced superconductivity in parent CaFeAsF single crystals. *Phys. Rev. B* **97**, 174505 (2018).